THE ASTROPHYSICAL JOURNAL, 555:31–39, 2001 July 1

UNDERSTANDING THE RADIO EMISSION GEOMETRY OF PSR B0329+54

R. T. GANGADHARA[1] AND Y. GUPTA[2]

Received 2001 January 10; accepted 2001 March 1

ABSTRACT

We have analyzed high-quality single-pulse data of PSR B0329+54 at 325 and 606 MHz to study the structure of the emission beam. Using the "window-threshold technique," which is suitable for detecting weak emission components, we have detected four additional emission components in the pulse window. Three of these are new components, and the fourth is a confirmation of a recently proposed component. Hence, PSR B0329+54 is now known to have nine emission components—the highest among all known pulsars. The distribution of the pulse components around the central core component indicates that the emission beam consists of four nested cones. The asymmetry in the location of the conal components in the leading versus trailing parts of the profile is interpreted as being due to aberration and retardation in the pulsar magnetosphere. These measurements allow us to determine the precise location of the four conal rings of emission. We find that the successive outer cones are emitted at higher altitudes in the magnetosphere. Furthermore, for any given cone, the emission height at the lower frequency is found to be more than that at the higher frequency. The inferred heights range from $\sim$160 to $\sim$1150 km. The set of "active" field lines, from which most of the conal radiation appears to originate, is found to be confined to a region located within $\sim$0.5–$\sim$0.6 of the polar cap radius. We discuss the implications of our new findings to our understanding of the pulsar emission geometry and its impact on the emission mechanisms.

Subject headings: pulsars: individual (PSR B0329+54) — radio continuum: stars — stars: magnetic fields — stars: neutron

On-line material: color figure

1. INTRODUCTION

Radio wave emission from pulsars is believed to originate in the open field-line region of the polar cap of the neutron star. The size, shape, and location of regions of radio emission in the average profiles of pulsars are thus expected to reflect the arrangement of emission regions in the pulsar magnetosphere. Average pulse profiles exhibit a great diversity in shape, and their classification based on the number of emission components is a useful starting point for studying the emission characteristics of pulsars. Rankin (1983a, 1983b, 1990, 1993) has carried out such a detailed classification and has reached the conclusion that there are two kinds of emission components—core and conal—in pulsar profiles, which result from two distinct types of emission mechanisms. Furthermore, Rankin proposes that the conal components arise from two nested hollow cones of emission, which, along with a central core emission region, make up the complete pulsar emission beam. The actual profile observed for a given pulsar depends on the cut that the observer's line of sight makes through this emission beam. From the above work, Rankin also concludes that core radiation originates from close to the neutron star surface, whereas the conal radiation originates in regions higher up in the magnetosphere. The outer cone is postulated to originate higher up in the magnetosphere than the inner cone but along the same set of field lines. However, there are other reports (e.g., Gil 1991) that postulate that the core and conal emissions might originate at very similar heights in the magnetosphere.

Lyne & Manchester (1988) also confirm the difference in properties between the core and conal emissions. However, they believe that emission within the beam is patchy; i.e., the distribution of component locations within the beam is random rather than organized in one or more hollow cones. They have come to the conclusion that a single emission mechanism can account for both the central and outer components. Furthermore, they propose that the observations are best described by a gradual change in the emission characteristics from the axial region to the outer edge of the emission beam rather than by two distinct emission processes.

In this paper we present the results from an analysis of emission components of PSR B0329+54. This pulsar, one of the strongest known at radio wavelengths, is an excellent laboratory for a detailed study of pulsar emission physics. The simplest radio observations of this pulsar show a profile with three clearly visible components, and in the classification scheme of Rankin (1990), it is identified as a "triple (T)" profile. The central component is thought to be due to core emission, and the two outer components are of the conal type. However, there has been some evidence for the presence of more than three distinct components for this pulsar. For example, Hesse (1973) has adopted five components for a study of the relative intensity variations between the different components. More recently, Kuzmin & Izvekova (1996), from a study of fitting Gaussians to distinct emission components in the average profile, have found that a five-component model does not adequately describe this pulsar's profile. They propose a six-component model and thereby question the validity of the core-cone structure of the emission beam. Hence, the detection of the correct number of emission components and their distribution with respect to the pulse longitude plays a crucial part in deciding whether the pulsar emission beam is conal or

[1] Indian Institute of Astrophysics, Kormangala, Bangalore, 560034, India; ganga@iiap.ernet.in.

[2] National Centre for Radio Astrophysics, TIFR, Pune University Campus, Post Bag 3, Ganeshkind PO, Pune, Maharahtra 411007, India; ygupta@ncra.tifr.res.in.

patchy. For PSR B0329+54, this attempt is further complicated by the fact that this pulsar is a mode changer; i.e., it switches between the two different modes of average profile (Lyne 1971; Hesse, Sieber, & Wielebinski 1973), during which time there is an appreciable change in the relative strengths and the locations of the emission components.

In this paper we present the results from an analysis of single-pulse data of PSR B0329+54 at two different frequencies. We have used the "window-threshold" technique, which is suitable for the detection of weak emission components in pulsar profiles (Gangadhara 2000). In § 2 we report the detection of new emission components in the profile of PSR B0329+54. In § 3 we interpret the results in terms of aberration and retardation effects in the pulsar magnetosphere and use this to estimate the emission heights and polar cap locations of the cones. In § 4 we discuss the implications of our findings on the structure of the emission beam of this pulsar.

2. OBSERVATIONS AND DATA ANALYSIS

For our study of the emission components of PSR B0329+54, we considered two data sets: the first obtained at 606 MHz from the Lovell telescope at Jodrell Bank and the second obtained at 325 MHz from the Giant Metrewave Radio Telescope (GMRT) at Khodad, India. Table 1 summarizes the main observing parameters for these data sets. The details of the observing system and the calibration procedures for the Lovell telescope are identical to those used by Gould & Lyne (1998).

For the GMRT, which consists of 30 antennas each with a 45 m diameter (see Swarup et al. 1997 for details), the data were obtained by the incoherent addition of the dual-polarization signals from six antennas. The bandwidth used was 16 MHz divided into 256 spectral channels by the digital back ends (see Gupta et al. 2000 for more details about the pulsar mode of operation of the GMRT). The raw data were integrated to a time resolution of 0.516 ms before being recorded for off-line analysis, in which the data were dedispersed and gated to obtain the single-pulse data. During off-line analysis, care was taken to check the data for radio frequency interference signals and to filter out the power-line frequency signals. The final 2100 pulses were collected from more than one observing session, each of which had the same observing parameters. For all the data sets from GMRT and Lovell, the profiles were aligned by defining the peak of the central component in the average profile as the location of zero-pulse longitude.

The average pulse profiles obtained from the 325 and 606 MHz data are shown in Figures 1*a* and 1*b*, respectively. For the Lovell data, the pulsar showed a mode change in the midst of the observations. In the beginning, for about 600 pulses, it was in the abnormal mode, after which it switched to the normal mode. The dotted curve in Figure 1*b* shows the average profile when the pulsar was in the abnormal mode. All the profiles in Figure 1 show five distinct emission components whose peaks lie in the longitude range of $-14°$ to $10°$. However, a study of the single pulses reveals the presence of significant emission outside these longitude ranges. For example, Figure 2*a* shows a sequence of about 300 pulses from the abnormal mode duration, where occasional emission in the longitude ranges from $-20°$ to $-16°$ and from $13°$ to $18°$ can easily be seen. This extra emission can also be detected in the average profile made from these pulses (Fig. 2*b*).

Since the pulses that have emission in the longitude ranges from $-20°$ to $-16°$ and from $13°$ to $18°$ are less frequent, these emissions are not clearly seen in the average

TABLE 1

SINGLE-PULSE OBSERVATIONS OF PSR B0329+54

Telescope	Date	Frequency (MHz)	Pulses	Resolution (ms)	Bandwidth (MHz)
GMRT.....	1999 Mar/Apr	325	2100	0.516	16
Lovell	1996 Aug 30	606	2500	0.249	40

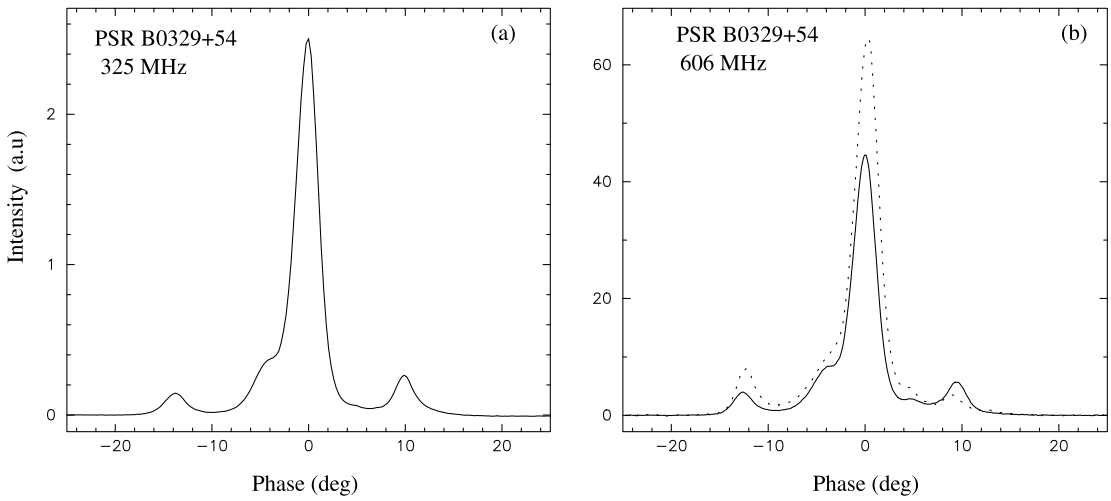

FIG. 1.—Average pulse profiles for PSR B0329+54 obtained from the data at 325 and 606 MHz. The intensity is in arbitrary units. For the 606 MHz data, the dotted curve shows the profile for the abnormal mode of the pulsar.

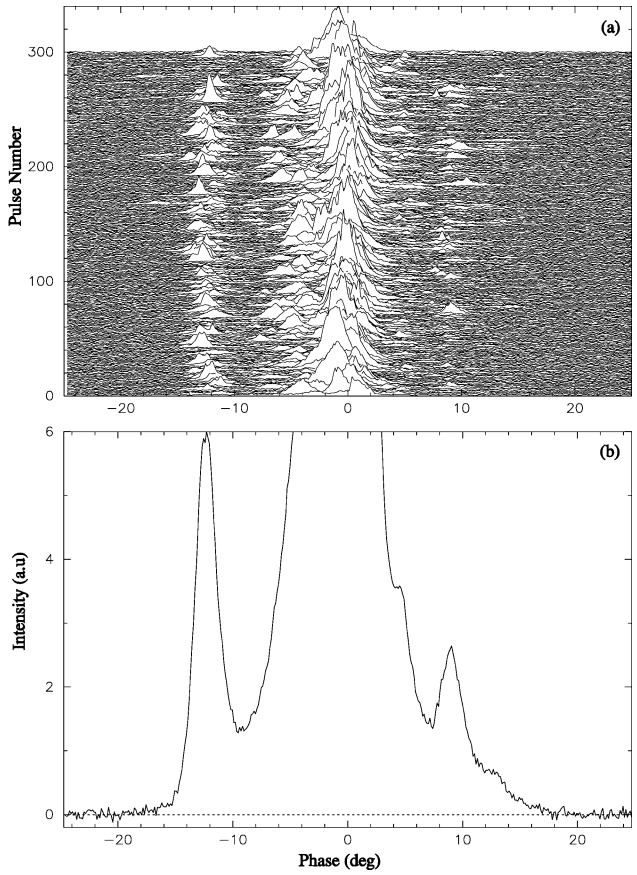

FIG. 2.—(*a*) Sequence of single pulses from PSR B0329+54 at 606 MHz; (*b*) average pulse profile obtained from the same frequency plotted with a zoomed intensity scale to enhance the emission at the outer longitudes. The dotted line shows the mean off-pulse intensity level.

pulse profiles in Figure 1. To enhance and easily detect emission from such regions, we have used a window-threshold technique (Gangadhara 2000) in which we set a window in longitude domain and employ an intensity threshold to select the single pulses that make an average profile. We consider all those pulses that have emissions above the threshold within the window. As a result of this averaging of selected pulses, the emission components within the window improve in signal-to-noise ratio compared to other parts of the profile and are more easily detected. Thus, for example, by setting a window over the longitude range from -20° to -16° and considering all those pulses that are above a 4 σ intensity threshold (here, σ is the rms of the intensity in the off-pulse region), we obtained an average profile shown as profile 8 in Figures 3*a* and 3*b*. This profile clearly shows an emission component (labeled component VIII in the figures) centered at about -18° for the 606 MHz data and at about -20° for the 325 MHz data.

The uniqueness in the phase location of a component peak (within error bars) with respect to the changes in the window position and threshold levels was used as a criterion for deciding whether a given pulse component was detected. As an additional criterion, we also looked at its detection at other frequencies and whether it follows the general trend of radius-to-frequency mapping followed by the known components.

By applying the technique repeatedly at different pulse longitude windows, we have determined the presence of nine unique emission components, shown by the nine average profiles in Figures 3*a* and 3*b*. The combined profile (Figs. 3*c* and 3*d*), obtained by adding all nine of these profiles, shows the relative location of the nine emission components of PSR B0329+54.

To test if this detection of components is unique, we have tried our window-threshold technique for choices of much broader longitude windows, such as those that enclose more than one component. In all such cases, our technique determines the same number and location of components. Furthermore, our technique detects no new components when applied to regions of longitude that are far away from the known on-pulse region. This argues that our detected components are genuine.

3. INTERPRETATION

Since we have identified eight conal components that are evenly distributed in number about the core component, our results can be interpreted in terms of a set of nested cones of emission. Figure 4*a* shows the location of the components in the form of four conal rings of emission around the core component for the 606 MHz data. In Figure 4*b* we show the pulse-phase extent of each cone at 325 and 606 MHz along with the location of the nominal center of the cone, taken to be the halfway point between the corresponding leading and trailing components. We estimate the phase location of any given component as the mean of the distribution of phases of the peaks of single pulses that are selected by our window-threshold technique. We estimate an error on this component phase location as the standard deviation of the same distribution. The error bar on the location (zero phase) of the core component is estimated to be about $\pm 0.^\circ 6$ at both the frequencies. We also estimated the component locations by fitting Gaussians to each component in Figures 3*a* and 3*b*, which gives the results that are the same within the error bars as the method we have adopted. From the plots in Figure 4, it is clear that the conal components are squeezed closer to the core (and to each other) in the trailing part of the profile as compared to the leading part. This asymmetry is clearly reflected in the shift of the cone centers away from the core and toward the leading part of the profile. This effect increases as we go from the inner cones to the outer ones. Furthermore, for the same cone, the effect is more pronounced at the lower frequency.

The above remarkable behavior has a simple interpretation: the radiation beams from the outer cones are progressively bent or deflected in the forward direction, i.e., the direction of the rotation of the pulsar. Such a bending can be produced by aberration and retardation effects in the pulsar magnetosphere (Cordes 1978). Below, we consider in detail the emission geometry in the pulsar magnetosphere and include the effects of aberration and retardation. Using these, we show that the emission heights as well as the transverse location of associated dipolar magnetic field lines on the polar cap can be uniquely estimated for each cone at each frequency of observation. We also consider the effect of magnetic field sweepback, which can produce a bending of the cones in the opposite direction. We find that in the present context, the effect of magnetic field sweepback is negligible compared to the aberration and retardation effects.

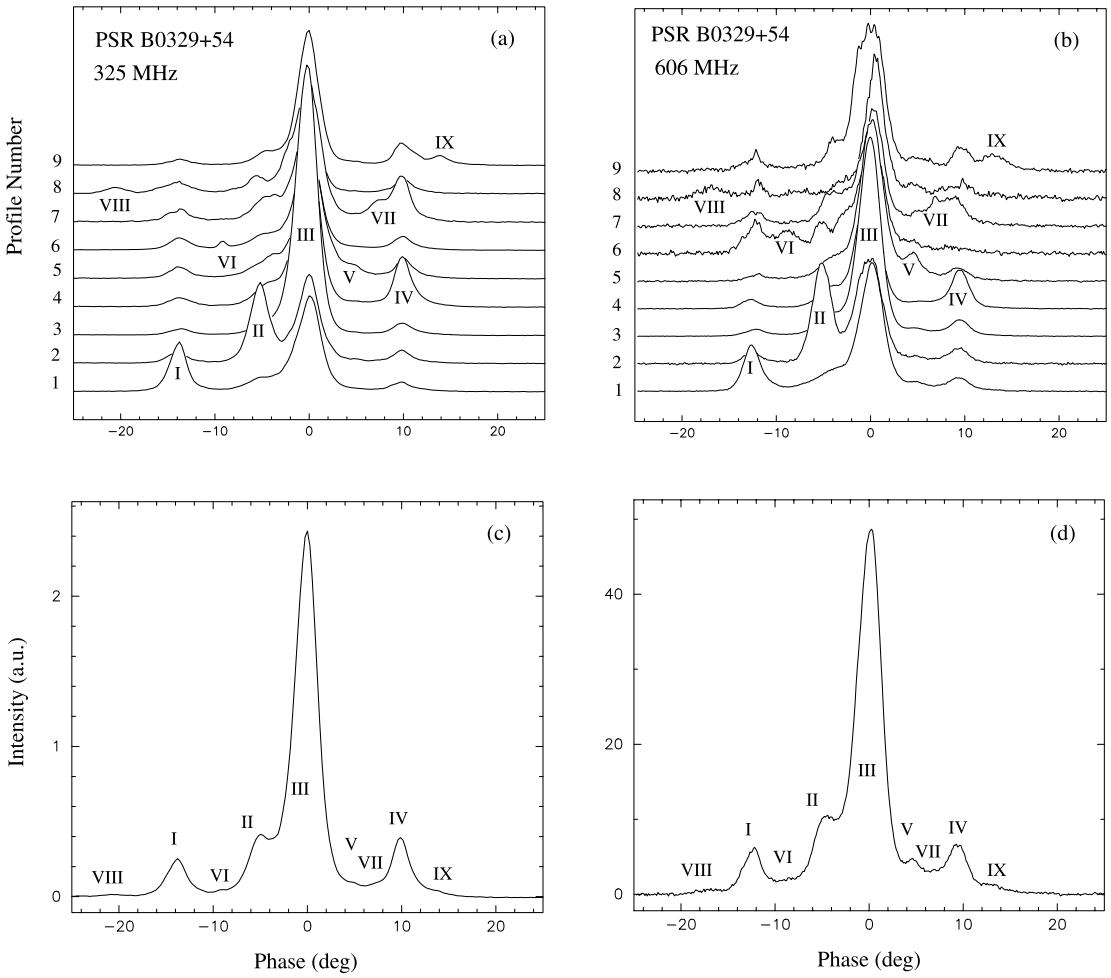

FIG. 3.—Panels (*a*) and (*b*) show the average profiles (in arbitrary units) obtained for each of the nine detected components using the window-threshold technique at 325 and 606 MHz, while panels (*c*) and (*d*) show the averages of these nine profiles.

3.1. *Emission Geometry*

The geometry relevant to our current understanding of the emission of radio radiation from the polar cap region of pulsar magnetospheres is illustrated in Figure 5. We start with a right-handed coordinate system originating at the center of the star with the z-axis aligned parallel to the rotation axis $\hat{\Omega}$. In the figure, $\hat{m}$ and $\hat{n}$ represent unit vectors along the magnetic axis of the pulsar and along the line of sight to the observer; they are inclined at angles α and ζ, respectively, to the rotation axis. The vectors $\hat{n}$, $\hat{m}$, and $\hat{\Omega}$ all lie in the x-z plane when the rotation phase $\phi = 0$. In this geometry, we have

$$\hat{n} = \hat{z}\cos\zeta + \hat{x}\sin\zeta\,, \tag{1}$$

$$\hat{m} = \hat{z}\cos\alpha + \sin\alpha(\hat{x}\cos\phi + \hat{y}\sin\phi)\,, \tag{2}$$

where $\zeta = \alpha + \beta$ and β is the impact angle of line of sight with respect to magnetic axis. The angle Γ made by $\hat{n}$ with respect to $\hat{m}$ at any ϕ is then given by

$$\cos\Gamma = \cos\alpha\cos\zeta + \sin\alpha\sin\zeta\cos\phi\,. \tag{3}$$

Now consider curve C in Figure 5, which represents a typical dipolar magnetic field line. Let p represent an emission point on this field line with spherical coordinates (r, θ) centered on the magnetic axis. Since the tangent to the field line at p needs to be parallel to $\hat{n}$, we can establish the following relationship between θ and Γ:

$$\tan\theta = -\frac{3}{2\tan\Gamma} \pm \sqrt{2 + \left(\frac{3}{2\tan\Gamma}\right)^2}\,. \tag{4}$$

This equation has two roots, and the continuous physical solution switches the sign of the second term on the right-hand side from positive to negative when Γ changes sign from positive to negative. For the region close to the magnetic axis, one can approximate equation (4) as $\theta \approx \frac{2}{3}\Gamma$.

Let $(r^i_{\rm em}, \theta^i_{\rm em})$ be the coordinates of the emission point for the ith cone (i = 1, 2, 3, and 4 are the cone numbers). In the absence of any aberration and retardation, it is assumed that the radiation from these points is emitted tangentially to the field lines. However, the aberration due to corotation causes emission beams to bend toward the azimuthal direction such that radiation is received earlier than if there were no rotation.

If ζ is the angle between the rotation axis and the line of sight, then the distance from the rotation axis to the line of sight is $r^i_{\rm em}\sin\zeta$. Hence, the rotation velocity at the emission point is $\Omega r^i_{\rm em}\sin\zeta$. If $v_{\|}$ is the velocity of particles along the field line, then the total velocity of particles $\boldsymbol{v}_{\rm tot} = \hat{b}v_{\|} + \hat{\phi}\Omega r^i_{\rm em}\sin\zeta$, where $\hat{b}$ and $\hat{\phi}$ are the unit vectors in the directions of the magnetic field and rotation, respectively.

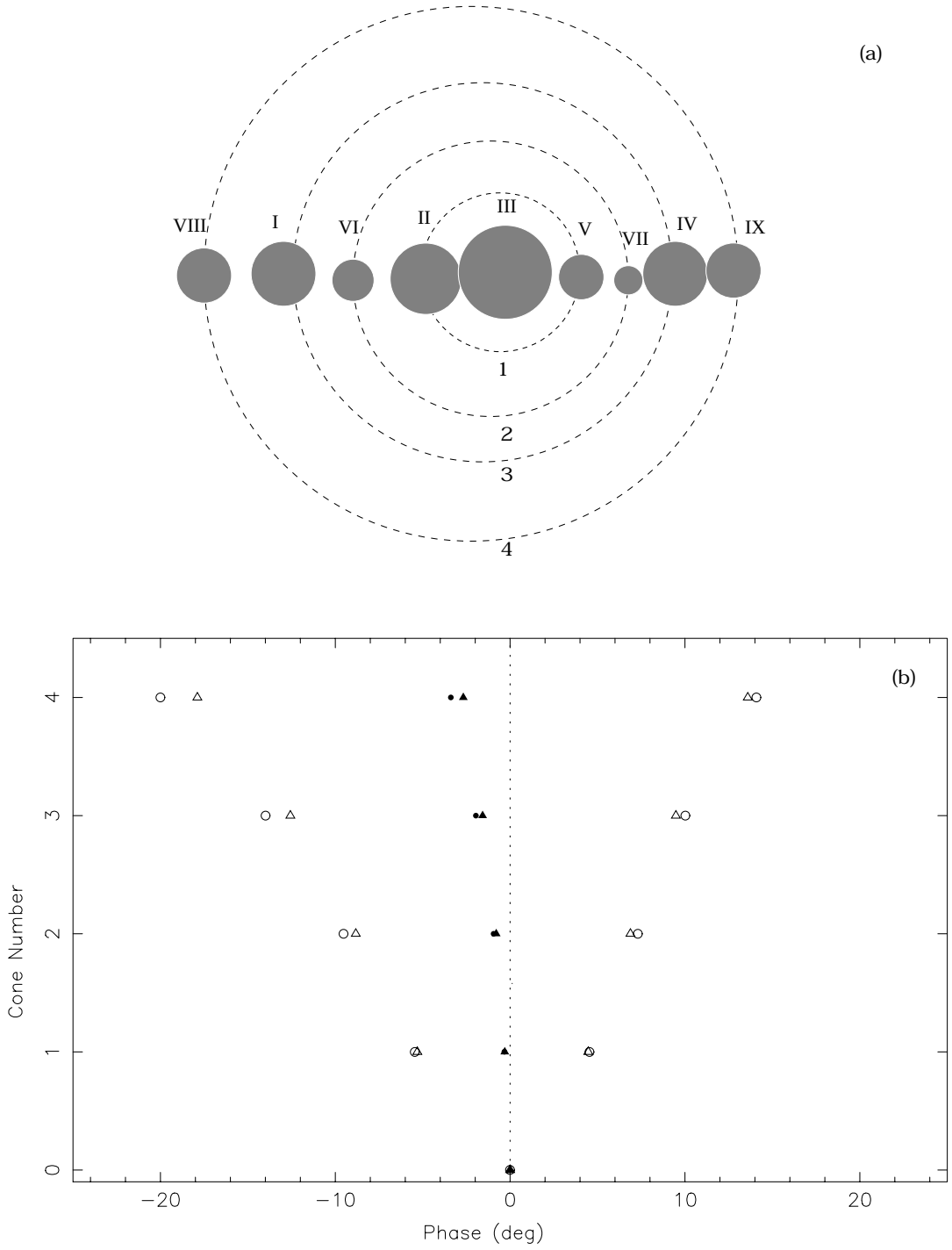

FIG. 4.—(*a*) Location of the nine emission components at 606 MHz shown in the form of four conal rings around the central core component; (*b*) extent (*open symbols*) and center (*filled symbols*) of the cones at 325 (*circles*) and 606 MHz (*triangles*). The core component is labeled as cone 0. Note that the scale for (*a*) is the same as that for (*b*). [*See the electronic edition of the Journal for a color version of this figure.*]

The aberration angle $\eta^i_{\rm ab}$ is given by

$$\sin \eta^i_{\rm ab} = \frac{\Omega r^i_{\rm em} \sin \zeta}{v_{\rm tot}} , \qquad (5)$$

where $v_{\rm tot} = |\boldsymbol{v}_{\rm tot}|$. It is more appropriate to assume $v_{\rm tot} \approx c$ instead of $v_{\parallel} \approx c$. Therefore, we have

$$\sin \eta^i_{\rm ab} = \frac{\Omega r^i_{\rm em} \sin \zeta}{c} = \frac{r^i_{\rm em}}{r_{\rm LC}} \sin \zeta , \qquad (6)$$

where $r_{\rm LC} = c/\Omega$ is the radius of the velocity of the light cylinder for the pulsar. Hence, the aberration is greater for emissions arising at larger altitudes.

Our aberration angle formula (eq. [6]) differs in the following two respects compared to the one given in the literature (e.g., Cordes 1978; Phillips 1992): (1) the literature formula uses α instead of ζ, which is correct only when the magnetic axis and the line of sight are aligned ($\beta = 0$), and (2) we estimate $\sin \eta^i_{\rm ab}$ instead of $\tan \eta^i_{\rm ab}$ since it avoids $v_{\rm tot}$ exceeding c when we set $v_{\parallel} \approx c$. However, the values of the

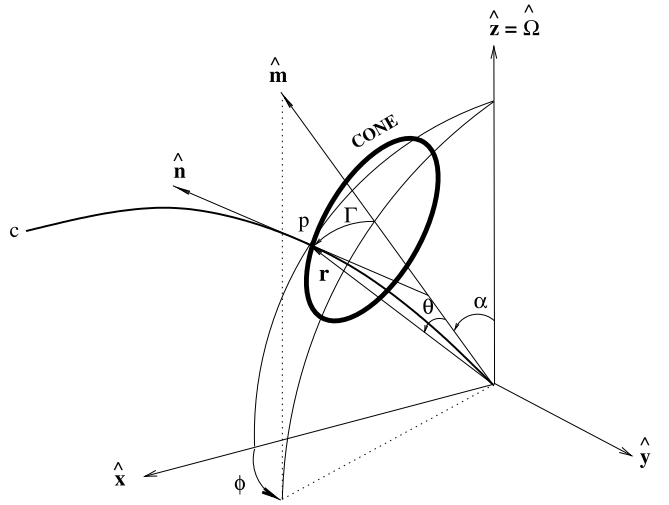

FIG. 5.—Emission geometry, where $\hat{n}$ is tangent to the dipolar field line c and directed toward the observer's line of sight, $\boldsymbol{r}$ is the position vector of emission point p, $\hat{m}$ is the magnetic axis, and ϕ is the pulse phase.

aberration angle estimated using the two formulae differ by a very little, i.e., on the order of $(r^i_{\rm em}/r_{\rm LC})^2$ for $\beta \ll \alpha$.

If the cones are emitted at different altitudes from the surface of the neutron star, then the conal radiation emitted at lower altitudes takes more time to reach the observer compared to the arrival times of those components emitted at higher altitudes. In terms of the pulse phase of the received radiation, this is equivalent to a shift of components emitted at a higher altitude to an earlier phase with respect to phases of lower altitude components. If $r^i_{\rm em}$ is the emission altitude of the ith cone, then this retardation phase shift is given by

$$\eta^i_{\rm ret} = \frac{r^i_{\rm em}}{r_{\rm LC}} \,. \tag{7}$$

The net phase shift due to aberration and retardation is $\eta^i = \eta^i_{\rm ab} + \eta^i_{\rm ret}$, which gives

$$\sin\left(\eta^i - \frac{r^i_{\rm em}}{r_{\rm LC}}\right) = \frac{r^i_{\rm em}}{r_{\rm LC}} \sin\,\zeta \,. \tag{8}$$

For the small-angle approximation ($\eta^i_{\rm ab} \ll 1$) , the solution of this equation is given by

$$r^i_{\rm em} \approx \frac{r_{\rm LC}\,\eta^i}{(1 + \sin\,\zeta)} \,. \tag{9}$$

Both aberration and retardation shift the pulse components emitted at higher altitudes to earlier phases in the received pulse. Therefore, we see an asymmetry in the location of the leading and trailing components with respect to the center of the profile. If ϕ^i_l and ϕ^i_t are the measured locations of the leading and trailing components, respectively, of a cone with respect to the center of the profile, then

$$\phi^i_l = -\phi^i + \eta^i \;; \quad \phi^i_t = \phi^i + \eta^i \,, \tag{10}$$

where ϕ^i is the phase of the ith component when the aberration and retardation are absent. From these, the values of η^i and ϕ^i are easily obtained:

$$\eta^i = \frac{(\phi^i_t + \phi^i_l)}{2} \;; \quad \phi^i = \frac{(\phi^i_t - \phi^i_l)}{2} \,. \tag{11}$$

The estimate of the net phase shift η^i, in conjunction with equation (8), immediately yields an estimate for the emission height $r^i_{\rm em}$ of the ith cone. Next, using the phase locations ϕ^i of the conal components, we can estimate the tangent angle Γ^i from equation (3) and the angular location $\theta^i_{\rm em}$ of the emission point from equation (4).

Furthermore, the knowledge of the emission height and angular location can be used to map the respective locations of the "footpoints" of field lines associated with the emission region of each cone on the polar cap. For this, we start with the equation of dipolar field lines

$$r = r_e \sin^2\,\theta \,, \tag{12}$$

where r_e is the field-line constant, which is the equatorial distance of a field line from the magnetic axis. Applying this at the surface of the neutron star gives

$$\frac{1}{r^i_e} = \frac{\sin^2\,\theta^i_s}{r_s} = \frac{\sin^2\,(s^i/r_s)}{r_s} \simeq \frac{s^{i2}}{r^3_s} \,, \tag{13}$$

where s^i is the distance from the magnetic axis to the foot of the field line (colatitude) as measured on the surface of a neutron star with radius r_s ($\sim$10 km). The approximate version in the above equation is for the case $\theta^i_s \ll 1$. At the emission point, the dipole field equation then yields

$$\frac{\sin^2\,(\theta^i_{\rm em})}{r^i_{\rm em}} = \frac{\sin^2\,(s^i/r_s)}{r_s} \,. \tag{14}$$

Under the small-angle approximation, we obtain the following relationship:

$$s^i \simeq s_L \sqrt{\frac{r_{\rm LC}}{r^i_{\rm em}}}\,\sin\,\theta^i_{\rm em} \,. \tag{15}$$

Here $s_L \approx (r^3_s/r_{\rm LC})^{1/2}$ is the distance from the magnetic axis to the foot of the last open field line that demarcates the polar cap region.

Using the above formulae, we have computed for PSR B0329+54 the emission heights and the location of the relevant field lines independently for each of the four cones and at each of the two frequencies. We have used $\alpha = 30^\circ$ and $\beta = 2^\circ\!.1$, as proposed by Rankin (1993) for this pulsar. Furthermore, we have taken the fiducial center point of the profile as the location of the core component, assuming that it is emitted at a very small height above the neutron star surface. Our results are summarized in Table 2 for the lower frequency (325 MHz) and in Table 3 for the higher frequency (606 MHz). The second and third columns give the measured locations of the leading and trailing components for each cone (with respect to the location of the core component), and the next two columns give the inferred values for the net phase shifts and tangent angles for the leading component of each cone. Column (6) gives the estimates of emission height (in kilometers) for each cone. Column (7) gives the estimates for the transverse location of the associated field lines on the polar cap. This is characterized by $s^i_L = s^i/s_L$. In the case of PSR B0329+54, the magnetic and rotation axes are inclined through an angle $\alpha = 30^\circ$; therefore, the polar cap is actually ellipsoidal with the major axis aligned in the longitudinal direction of the pulsar (Cordes 1978). For the purpose of normalizing, we consider the position of the last open field line, which is on the azimuthal direction $s_L \approx (r^3_s/r_{\rm LC})^{1/2} \sim 171$ m. The errors in component location are propagated appropriately to

TABLE 2

OBSERVED AND INFERRED LOCATIONS OF CONAL COMPONENTS AT 325 MHz

Cone (1)	ϕ_l^i (deg) (2)	ϕ_t^i (deg) (3)	η^i (deg) (4)	Γ^i (deg) (5)	$r_{\rm em}^i$ (km) (6)	s_L^i (7)
1.....	-5.5 ± 0.44	4.5 ± 0.29	-0.5 ± 0.26	3.3 ± 0.11	180 ± 100	0.5 ± 0.16
2.....	-9.5 ± 0.21	7.3 ± 0.31	-1.1 ± 0.19	4.8 ± 0.09	430 ± 070	0.5 ± 0.04
3.....	-14.0 ± 0.34	10.0 ± 0.42	-2.0 ± 0.27	6.5 ± 0.13	770 ± 110	0.5 ± 0.04
4.....	-20.0 ± 1.43	14.1 ± 0.72	-3.0 ± 0.80	9.0 ± 0.40	1150 ± 310	0.6 ± 0.08

estimate the errors for all other dependent parameters given in Tables 2 and 3.

The salient results from our interpretation of the emission geometry are as follows:

1. For the same cone, the lower frequency radio radiation is emitted at a higher altitude than the higher frequency radiation. This result supports the canonical picture of radius-to-frequency mapping.

2. For the same frequency, successive cones are emitted at higher altitudes in the pulsar magnetosphere. The heights range from nearly a hundred kilometers for the innermost cone to 1000 km for the outermost cone, or from about 0.5% to about 3% of the light cylinder radius.

3. *All* cones at *both* frequencies appear to originate on (or around) a narrow set of field lines slightly more than halfway out to the edge of the polar cap region ($s^i/s_L \approx 0.5$–0.6).

3.2. *Effect of Magnetic Field Sweepback*

We now consider the effect of magnetic field sweepback, an effect that opposes the aberration effect. Since pulsars lose their rotation energy by magnetic dipole radiation, the magnetic dipole field experiences a torque because of such emissions. As a result, the field lines tend to bend in the toroidal direction, which is opposite to the sense of rotation. To estimate the bending angle at the emission altitude $r_{\rm em}^i$, we use the following result given by Shitov (1983):

$$\phi_{\rm mfs}^i = 1.2\left(\frac{r_{\rm em}^i}{r_{\rm LC}}\right)^3 \sin^2 \alpha \, . \tag{16}$$

Using the emission altitudes given in the Table 2, we computed the bending angle due to field sweepback for each cone at each frequency and found that the sweepback is too small compared to the aberration and retardation phase shifts. For the outermost cone, where the sweepback is expected be highest, we find $\phi_{\rm mfs}^i < 0.^\circ001$ at 325 MHz and $0.^\circ0005$ at 610 MHz. Therefore, our assumption that the phase shifts of the cone centers with respect to the core position are predominantly due to the aberration and retardation is validated.

4. DISCUSSION

Our results show that PSR B0329+54 has nine unique emission components (of which at least three have been detected for the first time). This is the largest number of components detected for any pulsar and indicates that the emission geometry for this pulsar is probably quite complicated. We note that our component VI, detected in the longitude range from -8° to -10°, matches very well with the sixth component proposed by Kuzmin & Izvekova (1996) as a result of Gaussian fits to the emission components. Our results thus confirm the component proposed by them.

The new components are clearly seen at 606 MHz but are less prominent at 325 MHz. This may be part of the known trend of the reducing significance of conal components (with respect to the core component) at lower frequencies. Furthermore, the locations of components at the two frequencies follow the commonly seen trend that the distance from the center of the profile increases at lower frequencies, generally referred to as the "radius-to-frequency mapping" effect (see, e.g., Phillips 1992; Sieber 1996). This also supports the argument of the genuineness of the detected components. Our results also appear to indicate that the newly detected conal components for this pulsar show up more clearly during the abnormal mode rather than during the normal mode.

Our interpretation of the nine emission components as four nested cones of emission surrounding a single core component supports the picture of core and conal emission beams (see, e.g., Rankin 1983a; Oster & Sieber 1977). Rankin (1993) has proposed two conal rings to explain the existence of pulsars with five components in their average profiles. More recently, Mitra & Deshpande (1999) have found evidence for three nested conal rings from their analysis of the emission patterns of a large sample of pulsars. PSR B0329+54 is the first pulsar for which we found clear evidence for as many as four nested cones of emission. It should be interesting to see if a similar analysis

TABLE 3

OBSERVED AND INFERRED LOCATIONS OF CONAL COMPONENTS AT 606 MHz

Cone (1)	ϕ_l^i (deg) (2)	ϕ_t^i (deg) (3)	η^i (deg) (4)	Γ^i (deg) (5)	$r_{\rm em}^i$ (km) (6)	s_L^i (7)
1.....	-5.3 ± 0.35	4.5 ± 0.37	-0.4 ± 0.25	3.3 ± 0.10	160 ± 100	0.6 ± 0.17
2.....	-8.8 ± 0.34	6.9 ± 0.14	-1.0 ± 0.18	4.6 ± 0.08	380 ± 070	0.5 ± 0.05
3.....	-12.6 ± 0.64	9.5 ± 0.64	-1.6 ± 0.46	6.0 ± 0.22	600 ± 180	0.5 ± 0.08
4.....	-17.9 ± 0.79	13.6 ± 0.88	-2.2 ± 0.59	8.4 ± 0.29	840 ± 230	0.6 ± 0.09

for other multicomponent pulsars shows the presence of four emission cones.

Our data also present direct evidence for the detection of aberration and retardation effects in pulsar magnetospheres. Earlier experimental efforts to detect evidence for aberration and retardation time delays (as well as magnetic field sweepback) in some pulsars (e.g., Phillips 1992) did not yield any positive signature. Recently, Malov & Suleimanova (1998) estimated the aberration and retardation phase shifts for components I and IV of this pulsar using the average pulse profiles at different frequencies. The detection of aberration and retardation phase shifts of as much as 3° that we report supports the view that the conal emission originates at altitudes on the order of several hundred kilometers above the neutron star surface. Rankin (1993) reports an emission altitude of 217 km at 1 GHz for the main conal ring (cone 3 in our picture) of this pulsar. Kijak & Gil (1997, 1998) estimate somewhat higher emission altitudes, in the 300–500 km range. From our results, the corresponding emission altitude is about 600 km at 606 MHz.

Furthermore, the fact that a given conal ring exhibits more aberration at a lower frequency clearly shows that the lower frequency radiation originates at a higher altitude in the magnetosphere of this pulsar. This radius-to-frequency mapping effect has been proposed as an explanation for the commonly observed fact that the overall widths of pulsar profiles increase with decreasing frequency. Our results provide a direct corroboration of this model, and the results then make it less likely that other proposed explanations, such as chromatic aberration (or refraction) in the magnetosphere (see, e.g., Barnard & Arons 1986) or low-frequency broadening due to reduced beaming of the radiating particles (Kunzl et al. 1998), are valid.

By combining the emission heights obtained from aberration and retardation effects with a dipolar magnetic field geometry, we have been able to localize the exact emission point of each cone with a good degree of precision. Perhaps the most interesting result of our work is the conclusion that the successive cones of emission originate at increasing heights in the magnetosphere but along relatively nearby field lines. This is the first time that such a result has been obtained for any pulsar. In the context of two cones of emission, Rankin (1993) has raised the following major unanswered question: are the cones emitted at different heights along the same set of field lines or are they associated with different sets of field lines? For PSR B0329+54, this question is now answered for all four cones of emission. We find that all the cones at a given frequency are associated with a set of field lines that are located at about 0.5–0.6 of the distance to the edge of the polar cap. We believe that the scatter in the values (0.5–0.6) for different cones is within the limits of our estimation errors. Furthermore, we find that the cones at both frequencies are also associated with the same set of field lines, again within the error estimates.

We note, in particular, that our results show clearly that the radio emission does *not* originate at or near the last open field-line region of the pulsar magnetosphere. In the formulation we have presented in equations (1)–(15), there is only one free parameter that can affect this conclusion: the value of α, which is the inclination angle between the magnetic and rotation axes of the pulsar. Higher values of α would reduce the estimated emission heights and consequently move the associated field lines closer to the edge of the polar cap. However, there is good evidence that the value of $\alpha = 30°$ for this pulsar is a robust estimate (Rankin 1990; Lyne & Manchester 1988).

If the results about the emission geometry that we have obtained for pulsar B0329+54 are found to be true in general for the population of known pulsars, then it should prove to be a significant improvement in our general understanding of the emission geometry of radio pulsars. This could provide important constraints for the various theories for the emission mechanism of radio pulsars. For example, any successful theory would need to produce radiation at a given frequency from significantly different heights along the same set of field lines in the magnetosphere to explain the observed behavior of conal components.

5. CONCLUSION

We have used a technique based on windowing and thresholding to detect the weak emission components in pulsar profiles. By applying this to the single-pulse data of PSR B0329+54 at 325 and 606 MHz, we have detected three new emission components for this pulsar and also confirmed the presence of a new component proposed by Kuzmin & Izvekova (1996). We conclude that this pulsar has nine components, which is the highest among all the known pulsars.

We interpret the nine components as being produced by four nested hollow cones of emission along with a central core component of emission. Our results thus support the core and conal emission picture of pulsar radiation beams.

We find clear evidence that the conal components in the trailing part of the pulsar profile are squeezed closer to the core (and to each other) compared to the corresponding components in the leading part of the profile. We interpret this as evidence for aberration and retardation effects in the conal beams. The observed aberration and retardation phase shifts increase from the inner to outer cones, and for any given cone, the effect is more at the lower frequency.

From a detailed consideration of the emission geometry in the magnetosphere, including the effects of aberration and retardation, we are able to constrain the location of emission regions independently for each cone and at each frequency (325 and 606 MHz). From these computations, we are able to conclude the following: (1) for the same cone, the lower frequency radiation comes from a higher altitude than the higher frequency radiation; (2) for the same frequency, successive outer cones originate at higher altitudes; and (3) all cones at both frequencies appear to originate on (or around) a specific set of field lines that are located about halfway out to the edge of the polar cap region. The inferred emission heights for the cones range from ~ 160 to ~ 1150 km.

This is probably the first time that the emission regions corresponding to the conal components for a pulsar have been located so precisely and unambiguously. In particular, our conclusion that there is only a restricted region of the polar cap that is active in producing all the conal radiation that is observed should prove to be an interesting constraint for models or theories of pulsar emission mechanisms.

We thank Dunc Lorimer for his help in data reduction and fruitful discussions during the initial stages of the work. We are thankful to A. G. Lyne for providing the Jodrell Bank data and to J. M. Rankin, A. Peyman, and D. Mitra for useful discussions.

REFERENCES

Barnard, J. J., & Arons, J. 1986, ApJ, 302, 138
Cordes, J. M. 1978, ApJ, 222, 1006
Gangadhara, R. T. 2000, Bull. Astron. Soc. India, 28, 297
Gil, J. A. 1991, A&A, 243, 219
Gould, D. M., & Lyne, A. G. 1998, MNRAS, 301, 235
Gupta, Y., Gothoskar, P. G., Joshi, B. C., Vivekanand, M., Swain, R., Sirothia, S., & Bhat, N. D. R. 2000, in IAU Colloq. 177, Pulsar Astronomy: 2000 and Beyond, ed. M. Kramer, N. Wex, & R. Wielebinski (ASP Conf. Ser. 105; San Francisco: ASP), 277
Hesse, K. H. 1973, A&A, 27, 373
Hesse, K. H., Sieber, W., & Wielebinski, R. 1973, Nature, 245, 57
Kijak, J., & Gil, J. 1997, MNRAS, 288, 631
———. 1998, MNRAS, 299, 855
Kunzl, T., Lesch, H., Jessner, A., & von Hoensbroech, A. 1998, ApJ, 505, L139
Kuzmin, A. D., & Izvekova, V. A. 1996, in IAU Colloq. 160, Pulsars: Problems and Progress, ed. S. Johnston, M. A. Walker, & M. Bailes (ASP Conf. Ser. 105; San Francisco; ASP), 217
Lyne, A. G. 1971, MNRAS, 153, 27P
Lyne, A. G., & Manchester, R. N. 1988, MNRAS, 234, 477
Malov, I. F., & Suleimanova, S. A. 1998, Astron. Rep., 42, 388
Mitra, D., & Deshpande, A. A. 1999, A&A, 346, 906
Oster, L., & Sieber, W. 1977, A&A, 58, 303
Phillips, J. A. 1992, ApJ, 385, 282
Rankin, J. M. 1983a, ApJ, 274, 333
———. 1983b, ApJ, 274, 359
———. 1990, ApJ, 352, 247
———. 1993, ApJS, 85, 145
Shitov, Yu. P. 1983, Soviet Astron., 27, 314
Sieber, W. 1996, in IAU Colloq. 160, Pulsars: Problems and Progress, ed. S. Johnston, M. A. Walker, & M. Bailes (ASP Conf. Ser. 105; San Francisco: ASP), 167
Swarup, G., Ananthakrishnan, S., Subrahmanya, C. R., Rao, A. P., Kulkarni, V. K., & Kapahi, V. K. 1997, in High Sensitivity Radio Astronomy, ed. N. Jackson & R. J. Davis (Cambridge: Cambridge Univ. Press)